

# PCA detection and denoising of Zeeman signatures in stellar polarised spectra

M. J. Martínez González<sup>1</sup>, A. Asensio Ramos<sup>2</sup>, T. A. Carroll<sup>3</sup>, M. Kopf<sup>3</sup>, J. C. Ramírez Vélez<sup>4</sup>, and M. Semel<sup>4</sup>

<sup>1</sup> LERMA, Observatoire de Paris-Meudon, 5 place de Jules Janssen, 92195, Meudon, France  
e-mail: Marian.Martinez@obspm.fr

<sup>2</sup> Instituto de Astrofísica de Canarias, Vía Láctea S/N, 38200, La Laguna, Spain  
e-mail: aasensio@iac.es

<sup>3</sup> Astrophysikalisches Institut Potsdam, An der Sternwarte 16, 14482 Potsdam, Germany  
e-mail: tcarroll@aip.de

<sup>4</sup> LESIA, Observatoire de Paris-Meudon, 5 place de Jules Janssen, 92195, Meudon, France  
e-mail: Julio.Ramirez@obspm.fr, Meir.Semel@obspm.fr

Received ; Accepted

## ABSTRACT

**Aims.** Our main objective is to develop a denoising strategy to increase the signal to noise ratio of individual spectral lines of stellar spectropolarimetric observations.

**Methods.** We use a multivariate statistics technique called Principal Component Analysis. The cross-product matrix of the observations is diagonalized to obtain the eigenvectors in which the original observations can be developed. This basis is such that the first eigenvectors contain the greatest variance. Assuming that the noise is uncorrelated a denoising is possible by reconstructing the data with a truncated basis. We propose a method to identify the number of eigenvectors for an efficient noise filtering.

**Results.** Numerical simulations are used to demonstrate that an important increase of the signal to noise ratio per spectral line is possible using PCA denoising techniques. It can be also applied for detection of magnetic fields in stellar atmospheres. We analyze the relation between PCA and commonly used well-known techniques like line addition and least-squares deconvolution. Moreover, PCA is very robust and easy to compute.

**Key words.** Polarization — Stars: magnetic fields — Methods: numerical

## 1. Introduction

The light coming from most of the astrophysical scenarios is polarised. This radiation is usually described in terms of the Stokes parameters: the total intensity,  $I$ , the linear polarisation given by Stokes  $Q$  and  $U$ , and the circular polarisation given by Stokes  $V$ . The degree of polarisation is accounted for  $\sqrt{Q^2 + U^2 + V^2}$  which, in most cases, is very small compared to the total intensity. Several physical mechanisms related to the breaking of the spherical symmetry induce the generation of polarised radiation: scattering processes, the presence of magnetic fields through the Zeeman or Hanle effects, etc. For example, the presence of strong magnetic fields in solar or stellar spots produces a large degree of polarisation which, in some cases, can reach some tens percent. It decreases to  $\sim 0.01 - 0.1$  % in the less magnetically active areas of solar or stellar surfaces.

The investigation of the magnetic field in stellar atmospheres is restrained by the low expected and observed polarisation signals (e.g., Donati et al., 1997). In most cases the expected degree of polarisation is of the order or even below the noise level. This is specially critical when analysing the spectra of cool stars (Petit, 2007, and references therein), although this problem is already present for active stars. The most natural procedure to increase the signal to noise ratio ( $S/N$ ) is to increase the exposure time. However, it is limited by the rotation period of the star. A radically new solution to this problem was presented by

Semel & Li (1996) (see also Semel, 1989). They suggested to use multiline observations of the same star and combine the information of all of them to increase the sensitivity of the polarimetric observations. In the last decades, these ideas have been made possible thanks to the synergy between instrumental and theoretical advances. On the one hand, we have witnessed the development of very sensitive polarimeters attached to cross-dispersed Echelle spectrographs that produce data of very good scientific quality. Some examples of very successful instruments are ESPaDOnS<sup>1</sup> and NARVAL, both based on the concept of SEMPOL<sup>2</sup>. On the other hand, line addition techniques have permitted to take advantage of these large spectral range observations. An inflection point was the presentation of the Least-Squares Deconvolution (LSD) technique that allowed to detect polarisation signals in a broad variety of stars (Donati et al., 1997, 2007). The LSD technique is an improvement over the brute force line addition approach developed by Semel & Li (1996).

Although line addition techniques are very successful on the detection of the polarisation signatures in noisy spectra, they are based on very rough approximations. Another weak point is that the final polarisation signature obtained after applying these techniques is difficult to interpret. It cannot be associated with a standard spectral line and any analysis based on the theory of polarised radiative transfer of spectral lines cannot be directly

<sup>1</sup> Echelle SpectroPolarimetric Device for the Observation of Stars

<sup>2</sup> SEMel POLarimeter

applied. For this reason, it would be desirable not to work with “mean” profiles but to take advantage of multiline observations to increase the  $S/N$  of individual spectral lines. This would make much easier to interpret the results because one would deal with standard spectral lines.

Following this idea, we present in this paper a denoising technique based on a multivariate statistics method called Principal Component Analysis (PCA). A first application of this technique on real observational data has been used by Carroll et al. (2008) for Zeeman-Doppler imaging of late-type stars. A technique based on PCA has been already proposed for increasing the signal to noise ratio of stellar polarised spectra by Semel et al. (2006). This technique uses a data base of synthetic stellar spectra to construct the so-called Multi Zeeman Signatures, profiles that result from the cross-correlation of the observed spectrum and the principal components of the synthetic data base. In this paper, we propose another different approach using the same statistical technique. It allows us to efficiently denoise stellar polarised spectra so that an increase of the  $S/N$  per individual spectral line is obtained using efficiently the information encoded in the whole observed spectrum. Consequently, since we use the observed stellar spectrum itself, our method is model-independent. Moreover, we denoise the whole spectrum keeping the information carried by the spectral lines, making them susceptible of more sophisticated radiative transfer analysis as compared to all previous techniques.

## 2. Principal Components Analysis

Principal Components Analysis (PCA; see Loève, 1955), also known as Karhunen-Loève transformation, is an algorithm that belongs to the field of multivariate statistics. Briefly, it is used to obtain a self-consistent basis in which the data can be efficiently developed. This basis has the property that the largest amount of variance is explained with the least number of basis vectors. It is useful to reduce the dimensionality of data sets that depend on a huge number of parameters. This very property has been used during the last decades with denoising purposes, and it constitutes the main core of the denoising technique that we propose for polarised spectra.

For the sake of simplicity, we focus from the beginning in our particular problem of polarised spectra. When a spectrograph is used to observe a spectral line formed in a stellar atmosphere, it is sampled at a finite number of wavelengths, a number that depends on the spectral resolution of the instrumental setup. However, it turns out that this number is usually much larger than the number of physical variables involved in the spectral line formation mechanism (Asensio Ramos et al., 2007). Moreover, if we observe the full Stokes vector, the number of wavelengths increases in a factor of 4, while the number of physical parameters typically increases more slowly. It is easy to understand that correlations between the observables exist. This is related to the fact that the presence of physical laws constrain the possible values that any observable can take. For instance, all the wavelength points tracing the continuum away from spectral lines roughly provide the same information about the physical conditions. Since the stellar continuum is typically formed in local thermodynamical equilibrium conditions, it can be characterized by a Planck function at a given temperature. Therefore, all the wavelength points are linked by the functional form of the Planck function.

Due to these intrinsic correlations that exist in the observables, when a spectral line is observed many times, or, in our case, several spectral lines are observed simultaneously, the

cloud of points that represent all spectral lines in the multi-dimensional space of the observables will be elongated in some particular directions. These directions are the so-called principal components and the data can be efficiently reproduced as a linear combination of vectors along them.

Let us assume that the wavelength variation of each Stokes profile ( $I$ ,  $Q$ ,  $U$ , or  $V$ ) of a particular spectral line is described by the quantity  $S_i^j$ . The index  $i$  represents the wavelength position while the index  $j = \{I, Q, U, V\}$  indicates the Stokes parameter. Each Stokes parameter is a vector of length  $N_\lambda$ , corresponding to the number of wavelength points. In the ideal situation, it would be advantageous to have  $N_{\text{obs}} \gg N_\lambda$  observations, so that the number of observed lines is much larger than the number of wavelength points used to sample each line. Thanks to the cross-dispersed capabilities of instruments like SEMPOL, ESPaDOnS or NARVAL, a huge number of spectral lines is obtained in one exposure when recording spectro-polarimetric data. This fact allows us to apply statistical techniques to capture the intrinsic behavior of the points in the  $N_\lambda$ -dimensional space and to use PCA to reduce its dimensionality.

We define  $\hat{O}$  as the  $N_{\text{obs}} \times N_\lambda$  matrix containing the wavelength variation of all the observed spectral lines. The principal components can be found as the eigenvectors of this matrix of observations. This means that the PCA procedure reduces to the diagonalisation of the matrix  $\hat{O}$ . Since we are requiring that  $N_{\text{obs}} \gg N_\lambda$  holds, this matrix is not square by definition. Moreover, even if one uses the Singular Value Decomposition (SVD; see, e.g., Press et al., 1986) to diagonalise  $\hat{O}$ , the dimension of the matrix can be so large that computational problems can arise. It can be demonstrated that the right singular vectors of the matrix  $\hat{O}$  are equal to the singular vectors of the cross-product matrix:

$$\hat{X} = \hat{O}'\hat{O}. \quad (1)$$

The matrix  $\hat{X}$  is the  $N_\lambda \times N_\lambda$  cross-product matrix and the superindex “t” represents the transposition operator. The same applies to the left singular vectors, which are also eigenvectors of the cross-product matrix  $\hat{X}' = \hat{O}\hat{O}'$ . The matrix  $\hat{X}'$  has dimensions  $N_{\text{obs}} \times N_{\text{obs}}$  and is typically much larger than the matrix  $\hat{X}$ . However, one description is the dual of the other and they are completely equivalent. The  $i$ -th principal component,  $\mathbf{B}_i$ , fulfills:

$$\hat{X}\mathbf{B}_i = k_i\mathbf{B}_i, \quad (2)$$

with  $k_i$  its associated eigenvalue. All the eigenvectors can be put together in the matrix  $\hat{B}$ . This matrix has dimensions  $N_\lambda \times N_\lambda$  and contains the eigenvectors as column vectors. Note that the cumulative distribution of eigenvalues

$$g_m = \frac{\sum_{i=1}^m k_i}{\sum_{i=1}^{N_\lambda} k_i} \quad (3)$$

gives the relative amount of variance explained by the first  $m$  eigenvectors. Since these vectors constitute a basis, the observations can be written as a linear combination of them as follows:

$$\hat{O} = \hat{C}\hat{B}', \quad (4)$$

being  $\hat{C}$  the  $N_{\text{obs}} \times N_\lambda$  matrix of coefficients. The element  $C_{ij}$  of this matrix represents the projection of the observation  $i$  on the eigenvector  $j$ . This matrix can be easily calculated as:

$$\hat{C} = \hat{O}\hat{B}. \quad (5)$$

Note that the transposition operator of the matrix of the eigenvectors in Eq. (4) replaces the inverse operator because the matrix of singular vectors is orthogonal, so that it fulfills  $\hat{B}^{-1} = \hat{B}'$ .

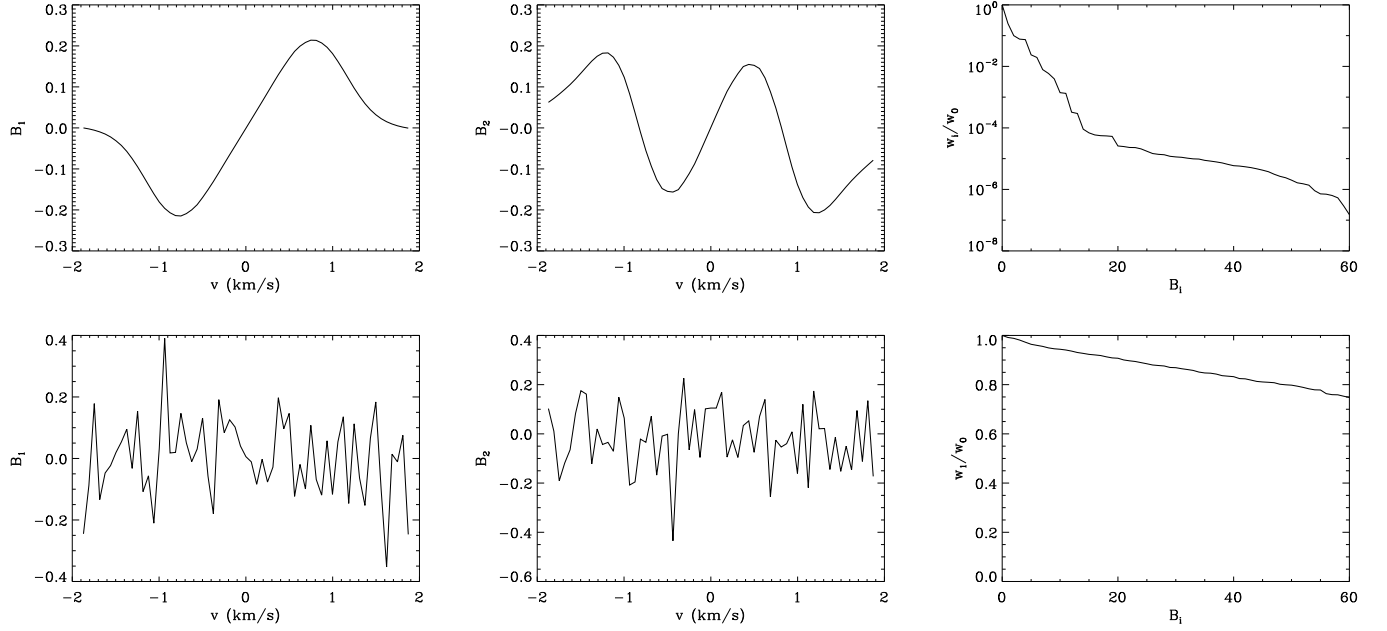


**Fig. 1.** Top panels: first (left) and second (centre) eigenvectors of the matrix of observations without any noise added. The dataset is described in Section 3.1. The right upper panel represents the eigenvalues for all the eigenvectors. Bottom panels: equivalent to the upper panels but for an observation containing only gaussian noise. The standard deviation of the distribution of noise is  $10^{-3} I_c$ .

This greatly simplifies the calculations because no numerical matrix inversion is needed.

### 3. Denoising procedure

In the following, we explain the procedure that we propose for denoising the experimental Stokes profiles of magnetic stars. The method is general, it should be used not only to retrieve Stokes  $I$  and  $V$  but to obtain Stokes  $Q$  and  $U$  given the important information encoded in it (see, e.g., the series of paper starting with Landolfi et al., 1993).

#### 3.1. The simulated data set

In order to demonstrate the capabilities of the PCA denoising technique, we use a synthetic polarised spectrum, including Stokes  $Q$ ,  $U$  and  $V$ . We cover the wavelength range between 400 and 900 nm, with a spectral resolution of 50 mÅ. The synthetic spectrum has been obtained under the assumption of local thermodynamical equilibrium (LTE) using a standard solar model atmosphere (Fontenla et al., 1993), with a star-filling magnetic field of 1000 G. The inclination of the magnetic field with respect to the line of sight is  $45^\circ$  and its inclination is  $20^\circ$ . This produces polarization signals that are much larger than those observed in real cases. For this reason, we apply a filling factor  $f$  to our simulated spectra in order to end up with Stokes  $V$  amplitudes that are similar to the ones expected in some cool stars observations ( $\sim 10^{-4} I_c$ , being  $I_c$  the continuum intensity). We quantify the quality of the data (amount of information about the physical conditions in the regions of line formation available in the data) with the signal to noise ratio,  $S/N$ . Consequently, the filling factor turns out to be unimportant and it is only chosen so as to end up with amplitudes comparable to the observed ones. The influence of realistic surface magnetic field distributions on the capabilities of the denoising technique will be addressed by Carroll et al. (2008; in preparation).

The spectral range that we use in our denoising technique is very large (500 nm), so that there is a large difference between the Doppler width of lines in the red and in the blue part of the spectrum. This is because the Doppler width is proportional to the wavelength. In order to make the Doppler widths compatible for all wavelengths, we transform the wavelength axis into the following velocity axis:

$$v = c \log \frac{\lambda}{\lambda_{\text{ref}}}, \quad (6)$$

where  $c$  is the speed of light, the symbol  $\lambda$  represents the wavelength and  $\lambda_{\text{ref}}$  is a reference wavelength, which we choose to be 400 nm. This change of variables induces that all the lines have, to first order, the same Doppler width in the new axis. Differences may exist because the Doppler width depends on the atomic mass of each species and because it also depends on the temperature in the line formation region. However, we assume that these differences are of second order with respect to the wavelength dependence. Since this new axis has an irregular step size because the spectrum has been sampled regularly in a wavelength scale, we re-interpolate it to a velocity axis with a regular step using a standard linear interpolation procedure. We set the spectral resolution equal to 0.2 km/s. This is equivalent to assume that the spectral resolution is the same regardless of the wavelength.

The individual spectral lines that will be used for building the matrix  $\hat{O}$  will be extracted using fixed positions for the central wavelength. In this experiment, we have computed the positions of the spectral lines as the positions where the minimum of the intensity profile is found. In any case, standardized linelists have been developed for different stars depending on the spectral type (Donati et al., 1997). The results that we show in this paper have been obtained using a database with  $\sim 6300$  lines. In principle, the capabilities of the method might be improved by using databases with more spectral lines, provided that the added lines carry sufficient information. We set  $N_\lambda = 40$ , choosing 20

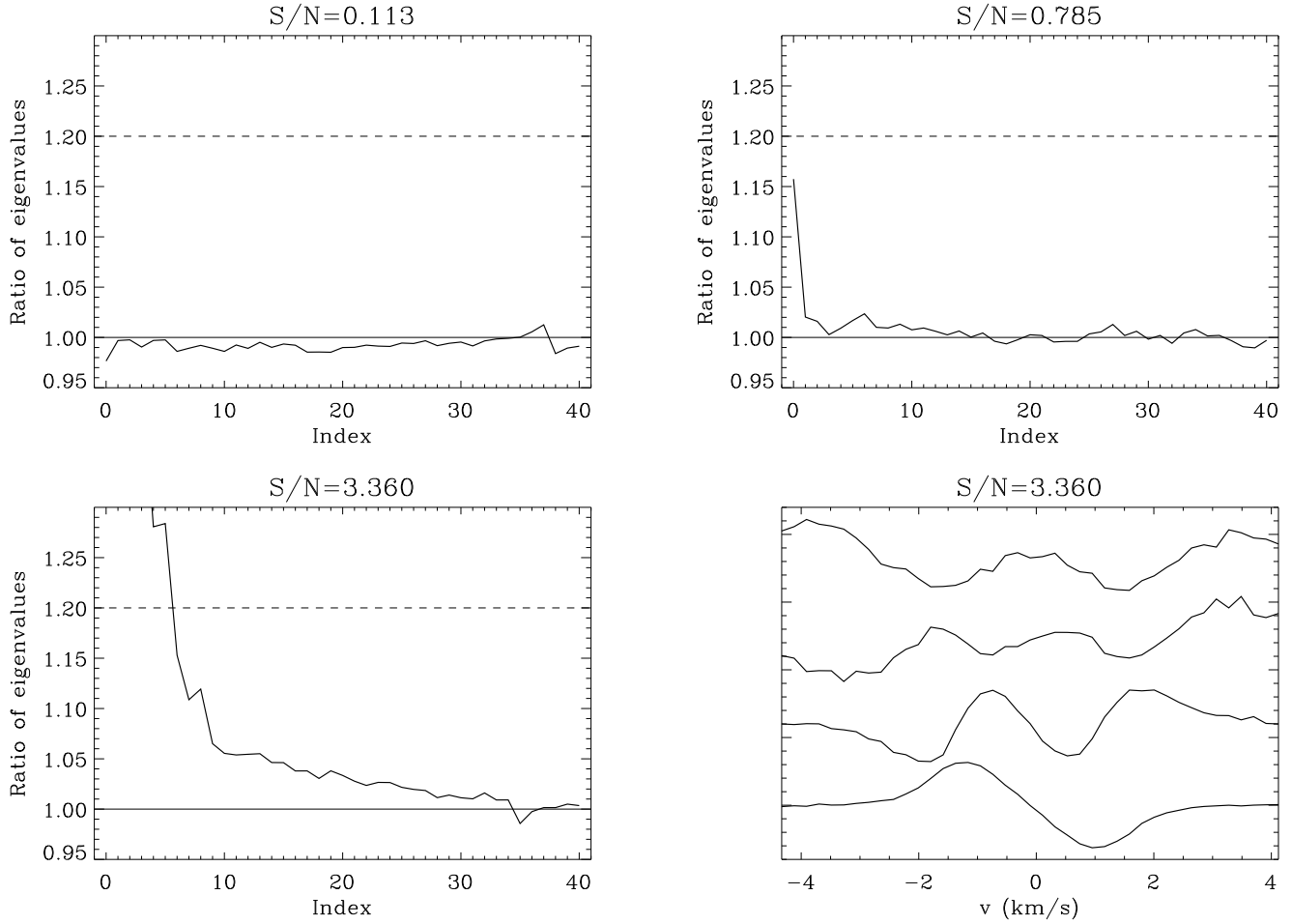


**Fig. 2.** Ratio between the eigenvalues of the noisy observations obtained for different  $S/N$  values and the ones of the pure noise observations (top and bottom left panels). The horizontal dashed line indicates the value  $f = 1.2$ . The bottom right panel shows the first four eigenvectors (ordered from bottom to top) for the case of  $S/N = 3.360$ . The eigenvectors are shifted in the vertical direction to avoid overlapping.

points to the red and 20 points to the blue. This translates into a velocity range of 8 km/s, which is sufficient for our experiment since we are not including the effects of rotation. In any case, in the analysis of a rapid rotator, a larger number of points have to be chosen. With each individual profile, we construct the matrix of observations ( $\hat{O}$ ) having one spectral line in each one of the rows.

### 3.2. Principal components of a “correlated” data set

We refer to a “correlated” data set when some correlation between the observables exist. In our particular case, this means that the physical mechanisms of line formation in stellar atmospheres introduce correlations between different wavelength points of each spectral line. The principal components of a correlated data set have some peculiarities that allow us to reduce the dimensionality of the data set. The principal components associated with the largest eigenvalues are representative of the directions of highest correlation and Eq. (3) can be used to estimate the relative amount of variance explained by them. Top panels of Fig. 1 show the first two eigenvectors of the matrix of observations of the Stokes V parameter without any noise added. The first eigenvector has the typical antisymmetric shape representative of the Stokes V profile induced by the Zeeman effect.

This means that the most important common pattern to all of our spectral lines resembles a Zeeman profile. Note also that the first eigenvalue is much larger than the following ones (right panel of Fig. 1; note the logarithmic scale). Although this is an expected result, note that we have not assumed in the analysis any systematic pattern in our data. On the contrary, it is a natural result of PCA. The rest of eigenvectors present other characteristics of the profiles whose importance decreases as the associated eigenvalue decreases.

The right panel of Fig. 1 shows that the first eigenvalues is the most representative one and that they drop dramatically. This is the key property of the PCA that allows us to reduce the dimensionality of the data set. This means that our observations can be efficiently reproduced using only a few eigenvectors. The observations were represented in a space of  $N_\lambda$  dimensions but the PCA analysis indicates that it is possible to represent them in a space of  $N'_\lambda$  dimensions (the number of chosen eigenvectors), with  $N'_\lambda \ll N_\lambda$ .

### 3.3. Principal components of uncorrelated noise

It is instructive to apply the same analysis based on principal components to a data set composed only of uncorrelated noise. In the limit  $N_\lambda \rightarrow \infty$  and  $N_{\text{obs}} \rightarrow \infty$ , the cross-product ma-

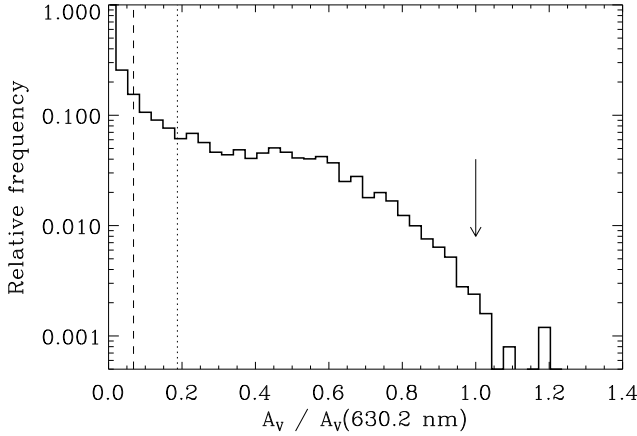


**Fig. 3.** Histogram of the amplitudes of the Stokes V profiles in the blue lobe divided the amplitude of the 630.2 nm spectral line. The histogram has been normalized to its maximum. The dashed line marks the position of the median value of the amplitudes while the dotted line shows the mean value. The arrows points to the value of 1 that corresponds to the 630.2 nm spectral line.

trix is strictly equal to the identity. As a consequence, the eigenvectors are the canonical basis and the eigenvalues are all equal to 1. However, since  $N_l$  is small, the cross-product matrix has non-diagonal elements and some spurious correlation may appear between different wavelength points. The bottom left and middle panels of Fig. 1 show the first two eigenvectors of a matrix with the same size as the one of the observations but containing only gaussian noise<sup>3</sup>. The gaussian distribution of noise has a standard deviation equal to  $10^{-3} I_c$ . All the eigenvectors are noisy, similar to those shown in the figure. The eigenvalues, represented in the bottom right panel of Fig. 1 are roughly the same for all the eigenvectors.

Real spectro-polarimetric measurements can present some degree of correlation between different wavelength points but are also contaminated by uncorrelated noise. Consequently, it is clear that the noise level will be an important issue that will restrain the denoising of the observations by means of principal components.

### 3.4. The procedure

To simulate the real case, we add gaussian noise to each spectral line of our matrix of observations. We apply the denoising procedure to our simulated data set with different values of added noise in order to analyze how it behaves in different situations. In order to use only one reference signal to noise ratio we choose the ratio between the polarisation signal ( $Q$ ,  $U$  or  $V$ ) in the magnetically sensitive 630.2 nm line and the standard deviation of the added noise distribution. Note that this  $S/N$  gives an idea of the quality of the data for the most magnetically sensitive lines, while the median of the  $S/N$  distribution is located at a much lower value, typically one order of magnitude smaller. This is produced by the fact that most of the lines induce small polarization signals, while only few lines give conspicuous signals.

<sup>3</sup> Note also that the random numbers obtained in computers are not strictly uncorrelated and this can induce (hopefully small) additional non-zero non-diagonal elements in the cross-product matrix.

Consequently, the distribution of amplitudes is strongly shifted towards zero.

For a given  $S/N$ , the eigenvectors of the cross-product matrix are computed as described in Section 2. If any systematic Zeeman signature is present in the dataset, it will appear in the first few eigenvectors. Since uncorrelated noise is also present in the observations (perhaps even completely masking the line polarization signals), the rest of eigenvectors having smaller eigenvalues contain the contribution of this noise. The filtering procedure consists on reconstructing the observed signal using only the first eigenvectors:

$$\hat{O}' = \hat{C}' \hat{B}', \quad (7)$$

where  $\hat{O}'$  is the matrix of observations after the denoising procedure. The matrix  $\hat{B}'$  contains the few first eigenvectors that have been retained as containing stellar magnetic signatures. The matrix  $\hat{C}'$  contains the coefficients of the projection of the matrix of observations onto the chosen basis of eigenvectors:

$$\hat{C}' = \hat{O} \hat{B}. \quad (8)$$

The selection of the number of eigenvectors that are dominated by polarimetric signal is the fundamental free parameter of the denoising procedure. It is not an easy task to efficiently select it and sometimes requires subjective criteria. We have verified that the following criterium works quite well for many of the tested cases and is also based on the properties of the PCA decomposition. For each value of the variance of the noise added to the simulated profiles, we compute an observation matrix equal to the observed one but made only of uncorrelated noise. In real situations, this matrix has to be built based on the estimation of the noise present in the observations. The eigenvalues of the pure noise matrix are calculated and compared with those of the real observations. If the variance of the noise has been correctly estimated, the two eigenvalue distributions will overlap except for those eigenvalues associated with correlated signals. Consequently, we select those eigenvectors  $b_i$  with eigenvalues higher than a factor  $f$  of those corresponding to the pure noise case. We have verified that  $f \approx 1.2$  gives good results. It is also instructive not to rely on automatic selection methods but verify the shape and weight of each eigenvector. The direct analysis of the eigenvectors can show many important details about the hidden signal and some tricks can be used to enhance the possibility of recovering it. A detailed discussion of the properties of the eigenvalues and the choice of the cutoff for the SVD problem can be found in Christensen-Dalsgaard et al. (1993) and in a series of papers by Hansen (1992), Hansen et al. (1992) and Hansen et al. (1993).

It is important to point out that the results we are presenting here are not the optimal case. For a field of 1000 G and since we do not include any additional line broadening mechanism, the majority of the lines are not in the weak field regime of the Zeeman effect. Therefore, they present different shapes (as a consequence of the Zeeman saturation) and part of the correlation is lost. We show that the PCA denoising technique is very performant in this non-optimal case. In stars with broadened lines (due to whatever mechanism), the weak field regime can be expected for larger magnetic field strengths and our PCA denoising algorithm will work even better.

In case none of the eigenvalues fulfill the criterium (to be expected in extremely noisy spectra), we have chosen to reconstruct using only the first eigenvector. The upper and bottom left panels of Fig. 2 show, for the cases discussed in the next section, the ratio between the eigenvalues of the cross-product matrix obtained from the synthetic data plus noise and the eigenvalues of

the pure noise cross-product matrix. The horizontal dashed line indicates the threshold that we choose to select the eigenvectors. The bottom right panel of the figure shows the first four selected eigenvectors for the less noisy case that we analyze in this paper.

## 4. Results

We present in this section the behavior of the PCA denoising in several  $S/N$  regimes. We range from very noisy profiles in which the signal is completely masked by the noise to less noisy profiles in which the PCA technique can be used to improve even more the quality of the data for the analysis of individual spectral lines. For the sake of simplicity, all the figures showing individual line profiles present results for Stokes  $V$ , although similar results (for similar values of the  $S/N$ ) are obtained for Stokes  $Q$  and  $U$ . However, the general denoising trends are presented both for circular and linear polarisation states.

### 4.1. Intermediate $S/N$

As representative of an intermediate  $S/N$ , we present the results obtained when the  $S/N$  in the 630.2 nm line is 3.358. As can be seen in Fig. 3 amplitudes like the one of the 630.2 nm are not very common in the spectrum. This means that most of the spectral lines would have  $S/N$  values at least 5 to 10 times smaller. Then, we are dealing with an example that can be representative of a typical observational case in stellar polarised spectra.

Although the real signal is still below the noise level for most of the lines, the number of selected eigenvectors is 4 according to the criterium of Sec. 3.4. The left panels of Fig. 4 show the comparison between the original synthetic profile without noise and the profile recovered after PCA denoising starting from the noisy profiles. The right panels of Fig. 4 show the comparison between the noisy and the PCA-filtered signals of three individual Fe I spectral lines and a Cr I line widely known in solar physics. In these conditions, the shape of all the spectral lines is roughly reproduced and the  $S/N$  of the filtered data is good enough for a reliable study of these individual spectral lines. The results presented so far have been obtained using the automatic criterium for the selection of eigenvectors to be included into the linear combination. This facilitates the statistical analysis of the method and gives an idea of how the methods behave with real data. However, we want to point out that better results are obtained in particular cases when one carefully selects the eigenvectors used to reconstruct the signal. An example of this is the lowest panel of Fig. 4, where the filtered signal has a spurious contribution from high-order PCA eigenvectors that can be improved by taking less PCA eigenvectors in the reconstruction.

Note that the results shown in Figs. 4, 5 and 6 correspond to a particular noise realization. The first eigenvector and the projection of the data onto it do change for different noise realizations (note also that the sign of the filtered profile can, in some cases, be the opposite to the original one). This will be explained in Section 4.4.

### 4.2. Low $S/N$

We present in this section the results when the  $S/N$  of the 630.2 nm spectral line has been decreased to 0.784. Figure 5 shows the comparison between the original and the filtered signals (left panels) and between the noisy and filtered observations for the same four spectral lines. According to the criterium presented in Sec. 3.4, we reconstruct the data taking into account

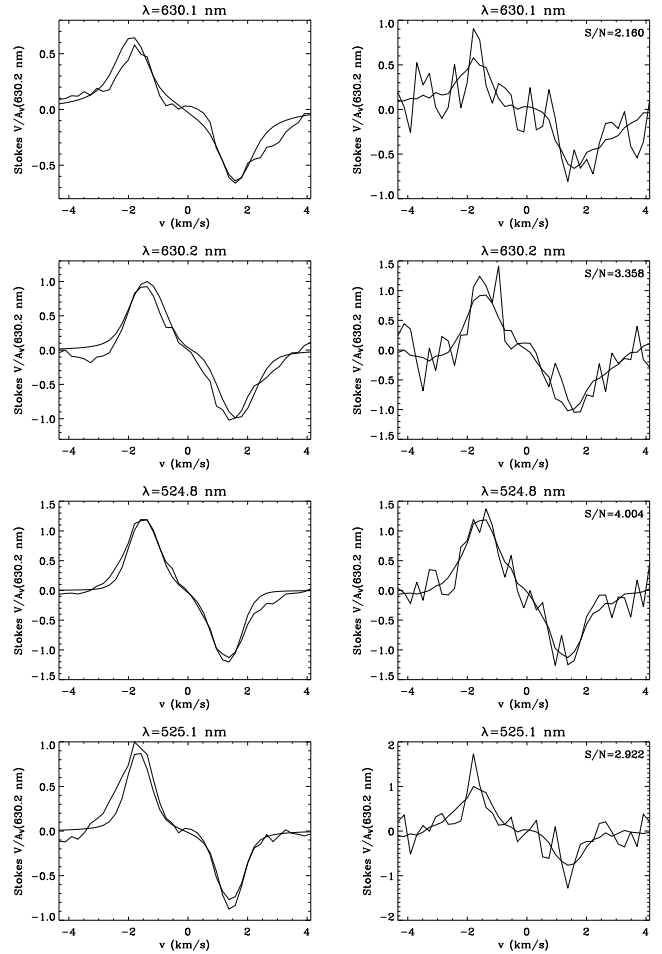


**Fig. 4.** Each row of this figure correspond to a particular spectral line. The first one is the Fe I line at 630.1 nm, the second one is the Fe I spectral line at 630.2 nm, the third one is the Cr I line at 524.8 nm, and the fourth one is the Fe I line at 525.1 nm. The amplitudes are normalized to the amplitude at the blue lobe of the 630.2 nm spectral line. Left panels represent the original profiles of each spectral line (thin line) and the filtered profiles (thick line). Right panels represent the noisy profile of each spectral line (thin line) and the filtered one (thick line). The  $S/N$ , taking the Fe I line at 630.2 nm as reference,  $S/N$  is 3.358. Note that the recovered Stokes  $V$  profiles are almost overlapping the original ones.

only the first eigenvector. This case is even worst than the typical scenario we can expect from real spectro-polarimetric observations (e.g., Donati et al., 1997). Fig. 5 shows that the  $S/N$  of the filtered data has been considerably improved. The shapes of the spectral lines can now be foreseen under the noise, mainly in the first and third panels. However, note that since we are taking into account only the first eigenvector, many details are still not reproduced. This means that all spectral lines should have the same shape, the only difference between them being the projection coefficient. However, the improvement in  $S/N$  has allowed to unambiguously detect the presence of circular polarization signals in some lines.

### 4.3. Very low $S/N$

As a representative of a case in which the signal is far below the noise level, we have chosen a noise distribution with a  $S/N$

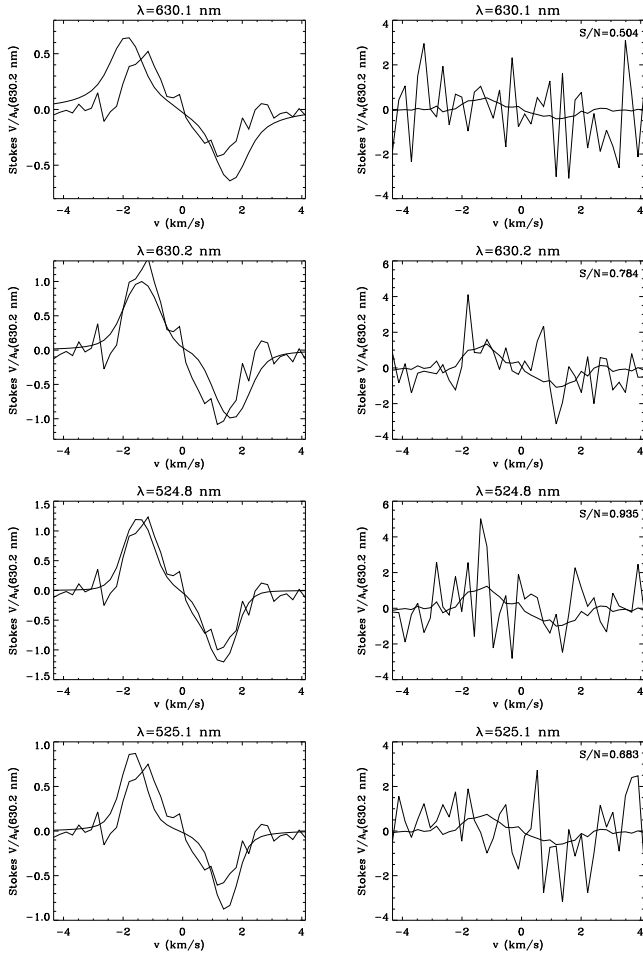


**Fig. 5.** The same as in Fig. 4 but for  $S/N$  is 0.784.

in the 630.2 nm line of 0.113. The signal to noise ratio in each individual line is indicated in each panel. Only the first eigenvector has been used for reconstructing the data set according to the criterium described above. It is evident that the signal has been strongly filtered and that the noise level is much lower than in the simulated observations. In this case, the value of  $S/N$  is so small that the information about the line profiles can not be extracted from the noisy data.

#### 4.4. Denoising trends in $S/N$

The lowest the noise level the largest the spectro-polarimetric information contained in the observations. Consequently, the  $S/N$  of the filtered data will be better if the  $S/N$  of the observations is not dramatically small. Of course, when the noise level in the observations is negligible, the filtering procedure leads to a small improvement. Figure 7 presents the general trend in the improvement of the  $S/N$  after the PCA denoising is applied. The same applies to Fig. 8 for the case of Stokes  $Q$ . The solid line in Fig. 7 shows the  $S/N$  of the filtered data versus the  $S/N$  of the observations. Again, we define the  $S/N$  of the filtered data as the ratio between the amplitude of the Stokes  $V$  amplitude of the 630.2 nm line ( $10^{-4} I_c$ ) and the standard deviation of the difference between the filtered and the original profile. In order to estimate the statistical significance of these values, we have estimated confidence intervals using a Montecarlo approach. The PCA denoising procedure has been applied to each line for 100 different

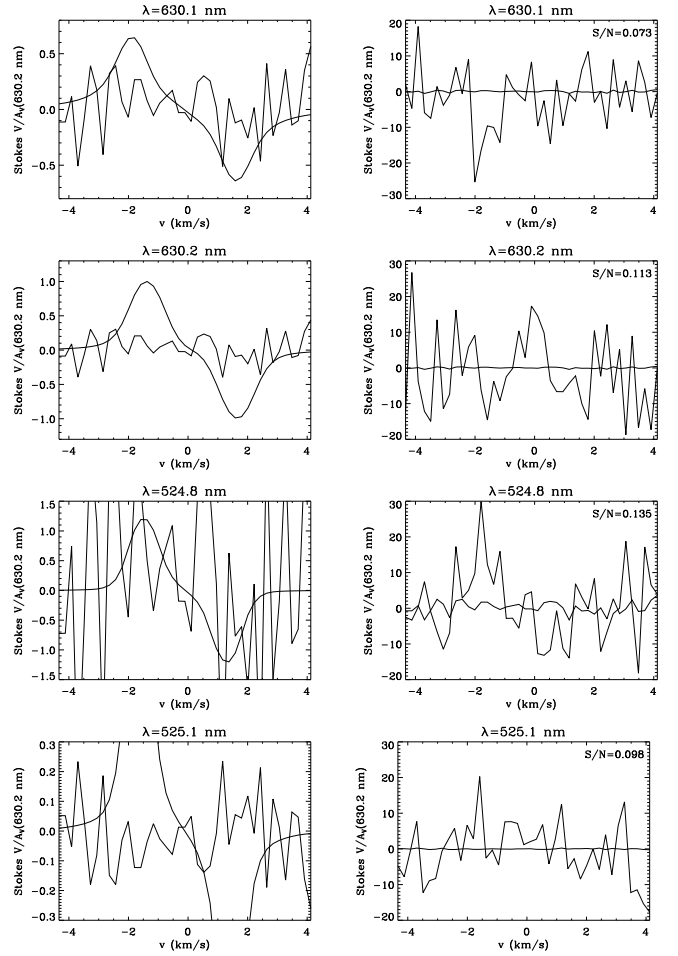


**Fig. 6.** The same as in Fig. 4 but for  $S/N$  is 0.113.

realizations of each individual standard deviation of the noise. The confidence intervals are obtained as the positions around the most probable value that enclose 68% of the probability.

Although the results are slightly different for each spectral line, they share the same behavior. If the  $S/N$  of the observations is below  $\sim 0.5$ , the amount of polarimetric information that we can extract from the spectrum is very small. Therefore, the analysis based on principal components is of reduced application. In this case, none of the eigenvalues of the cross-product matrix fulfill the selection criterium and we use only the first eigenvector with detection purposes. However, it is important to be cautious in this case, as already presented in Section 3.4. When the signal to noise is at least  $0.6 - 0.7$ , there is an improvement on the  $S/N$  of the filtered signal. For instance, note that with a  $S/N$  of 0.7 in the observations we increase it in almost one order of magnitude. Finally, as expected, if the noise level is very small we do not improve the  $S/N$  in the filtered data. Summarizing, as aparent from Figs. 7 and 8, the goal of having a  $S/N \sim 1$  can be accomplished with an observed spectrum with  $S/N \sim 0.1$ .

## 5. Connection with previous approaches

### 5.1. Line addition

The line addition technique (Semel & Li, 1996) consists of adding all the spectral lines together for equal velocity displacements from line center. The photon noise and the blends are supposed to add in an incoherent way and the polarimetric informa-

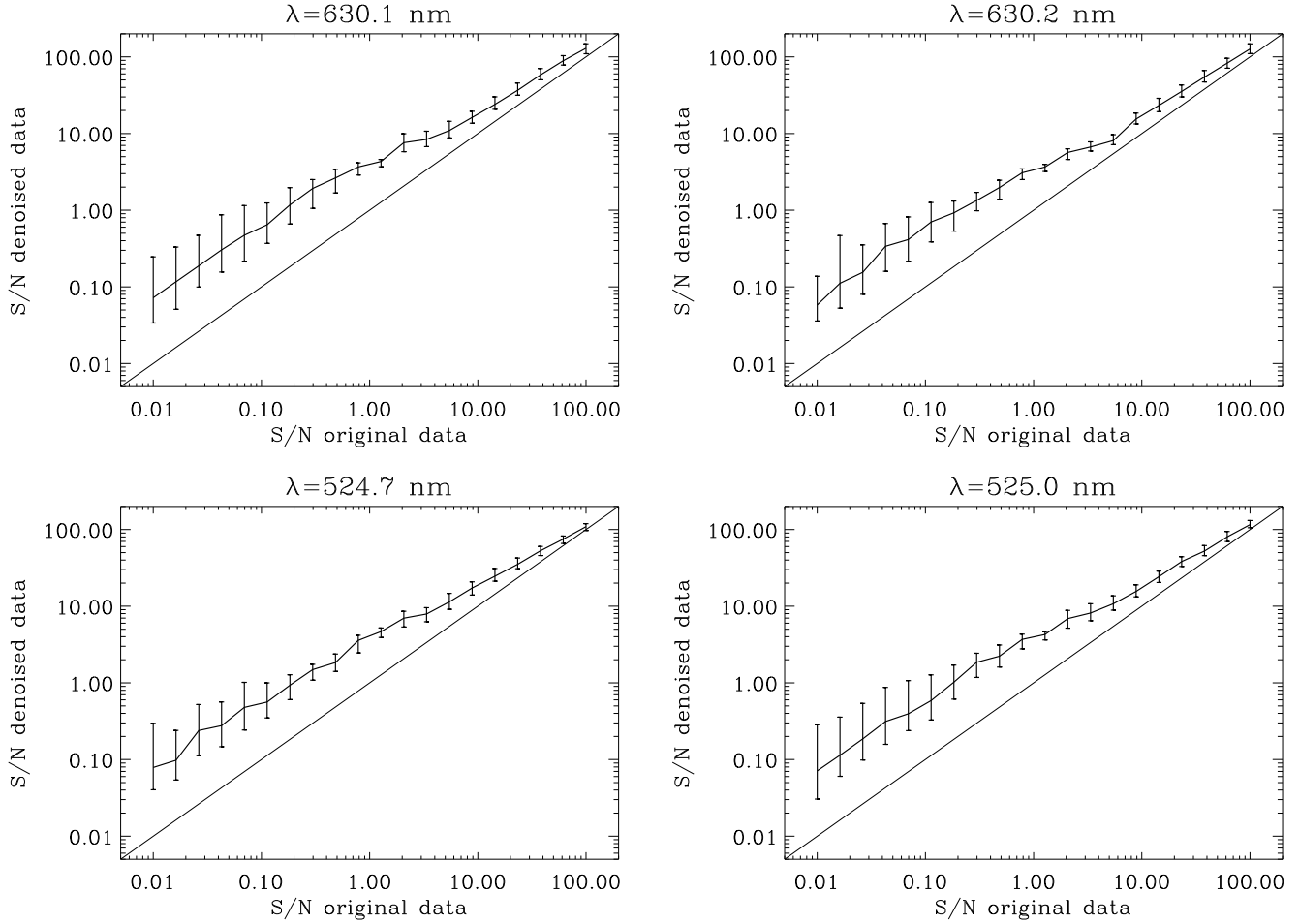


**Fig. 7.** Signal to noise ratio of the filtered data versus the original  $S/N$  of the observations for Stokes V. The error bars indicate the 68% confidence interval obtained in a Montecarlo procedure with different noise realizations.

tion is supposed to add coherently. Consequently, one ends up with a mean profile with a considerably higher  $S/N$ , an increase that is roughly proportional to the square root of the number of added lines. It is a very useful technique to detect polarisation in stellar spectra. The drawback is that the profile is difficult to analyze. The mean profile is not a spectral line because its behavior with the magnetic field is not the same as if it were a standard spectral line.

Under the PCA approach, it is also possible to retrieve the mean profile of the observations. The following expression, obtained after some simple algebra from Eqs. (4), gives the average profile  $\mathbf{P}$ :

$$\mathbf{P} = \frac{\sum_{jk} C_{jk} \mathbf{b}_k}{N_{\text{obs}}}, \quad (9)$$

where the index  $k$  indicates the eigenvector and  $j$  refers to the observation. The quantity  $C_{jk}$  is the projection of the observation  $j$  onto the eigenvector  $k$ . The previous analysis can also be done using only the first eigenvector. In this case, we end up with the most common pattern in the data. Since we are using the cross-product matrix (and not the covariance matrix in which the mean is subtracted from the observations), the following average profile (reconstructed using only the first eigenvector) is very close to the mean profile of Eq. (9):

$$\mathbf{P}_1 = \frac{\sum_j C_{j1} \mathbf{b}_1}{N_{\text{obs}}}. \quad (10)$$

The reason is that the first eigenvalue is the largest one and contains most of the variance of the data set. Then, as the eigenvalues drop rapidly, the rest of eigenvectors are much less important. The following analysis demonstrates that the PCA denoising can be made equivalent to the line addition technique, being also a suitable technique to detect magnetic signals in stars.

## 5.2. Least-Squares Deconvolution

The Least-Squares Deconvolution method presented by Donati et al. (1997) is a variation of the line addition. It is based on the following two hypothesis: the lines are assumed to be in the weak field regime of the Zeeman effect and there is a common pattern to all spectral lines. Since the lines are assumed to be in the weak field regime of the Zeeman effect, their Stokes V profiles are proportional to the longitudinal component of the magnetic field and the proportionality constant depends on the spectral line. This induces that the resulting LSD Stokes V profile is also linear in the longitudinal component of the magnetic field making the analysis possible in terms of a pseudo-line with an effective average Landé factor. The assumption that all the Stokes profiles of all the spectral lines are proportional to a common “mean Zeeman signature” reduces the problem to the following linear system of equations:

$$\mathbf{V} = \hat{\mathbf{W}} \mathbf{Z}, \quad (11)$$



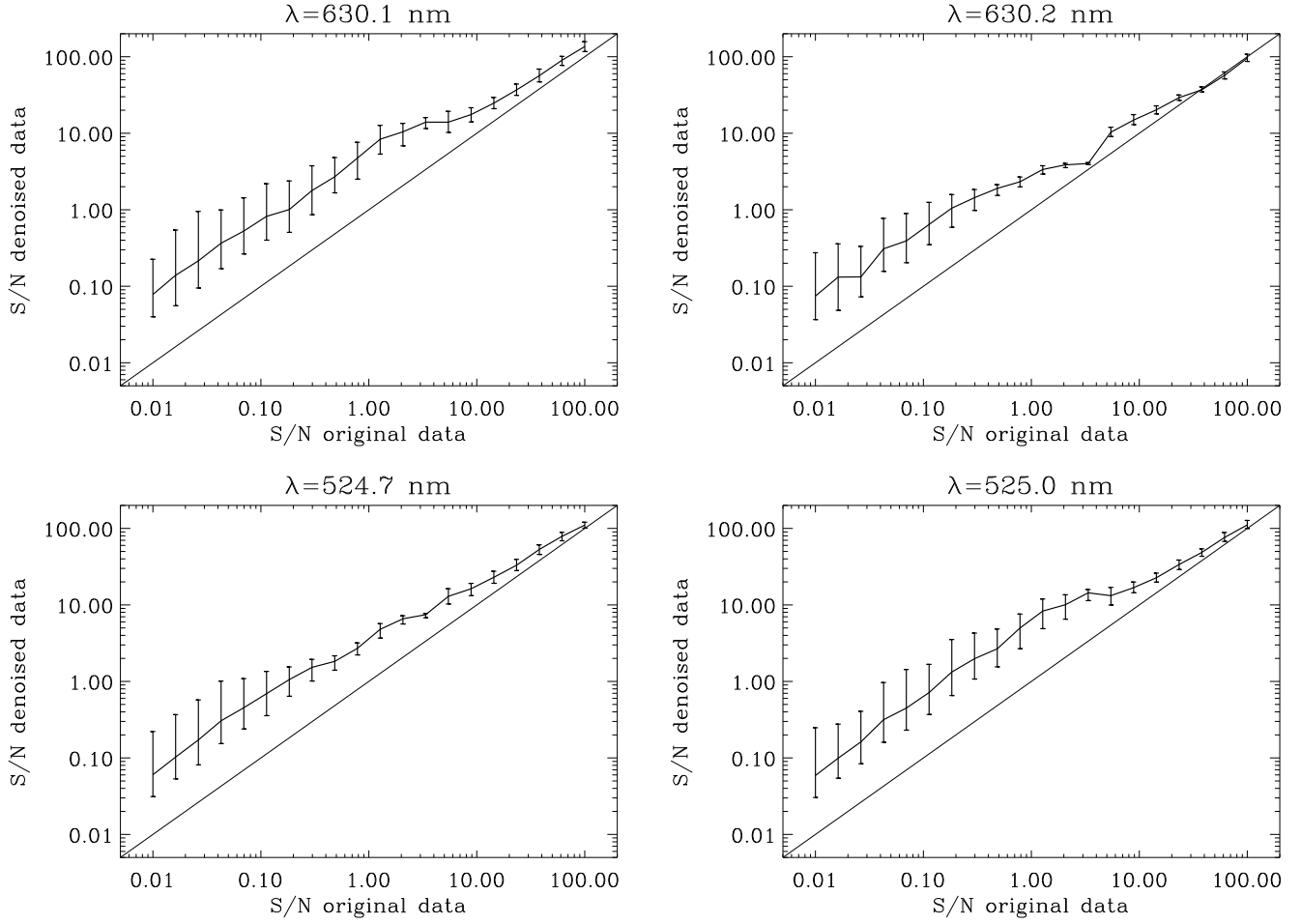


**Fig. 8.** Signal to noise ratio of the filtered data versus the original  $S/N$  of the observations for Stokes  $Q$ . The error bars indicate the 68% confidence interval obtained in a Montecarlo procedure with different noise realizations.

where  $\mathbf{V}$  is a vector of length  $N_{\text{obs}}N_{\lambda}$  containing the observed line profiles. The matrix  $\hat{\mathbf{W}}$ , of size  $N_{\text{obs}}N_{\lambda} \times N_{\lambda}$ , contains the weights  $w$  for each spectral line which, in this approximation, are defined by means of its Landé factor  $g$  and its central depth  $d$ :

$$w = g\lambda d. \quad (12)$$

The vector  $\mathbf{Z}$  is the so-called LSD profile, which is the characteristic Zeeman signature of the star. One of the weakest points of this technique is that the weights have to be proposed a priori. Once the weights are imposed, the linear system has the following least-squares solution:

$$\mathbf{Z} = (\hat{\mathbf{W}}^t \hat{\mathbf{S}}^2 \hat{\mathbf{W}})^{-1} \hat{\mathbf{W}}^t \hat{\mathbf{S}}^2 \hat{\mathbf{V}}, \quad (13)$$

where the matrix  $\hat{\mathbf{S}}$  is a diagonal matrix containing the inverse of the error bar of each spectral pixel. The previous solution is obtained using the weighted pseudo-inverse of the matrix  $\hat{\mathbf{W}}$ .

The examples shown in Figs. 6 and 5 are very close to what LSD represents because we use only the first eigenvector for the reconstruction. By so doing, we assume that all spectral lines can be reproduced by a common structure (the first eigenvector), the only difference between them being a scale factor (the projection of each observation along the first eigenvector). Instead of assuming the weight for each line, PCA naturally retrieves the common pattern in the observations and its intrinsic scale factor. However, note that the lowest the  $S/N$  the highest the dispersion

of the PCA coefficients. Then, for extremely low  $S/N$  we must be careful on the interpretation of this coefficient in terms of physical parameters.

PCA can be understood as a generalization of the basic idea of LSD in the sense that each spectral line is now a linear combination of several particular functions. In order to investigate the relation between PCA and LSD, we present in Fig. 9 a scatter plot showing the value of the first PCA coefficient and the LSD scaling factor, given by Eq. 12. This plot has been obtained for  $\sim 2000$  spectral lines without any noise added. Each spectral line can be contaminated with surrounding spectral lines in the same spectral range, inducing negative projections on the first PCA eigenvector. Also note that a reduced group of lines can have negative Landé factors, giving also negative projections on the first PCA eigenvector. The values are unimportant since both the amplitudes of the LSD profile and the first eigenvector are not equivalent. However, the plot shows no apparent correlation between the two coefficients. In this particular case, even if the concepts of PCA and LSD are similar, the stellar Zeeman profile retrieved with LSD is not the common pattern in the data (which is clearly the first eigenvector). In a strict mathematical sense, PCA is not directly related to LSD but to the more general Total Least-Squares (TLS; Huffel & Lemmerling, 2002). The standard linear least-squares method attributes all error to the dependent variables ( $\mathbf{V}$  in our case) and it minimizes the distance between the observations and the linear fit as measured along a particu-

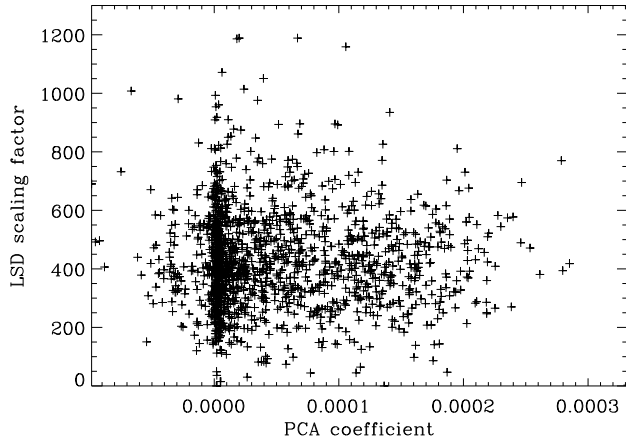


**Fig. 9.** Scatter plot showing the value of the projection of  $\sim 2000$  observed line profiles onto the first eigenvector versus the LSD scaling factor associated with each line.

lar axis direction. The weight matrix  $\hat{W}$  is assumed to be known without error. On the contrary, the linear TLS method allows errors in both the dependent and independent variables ( $V$  and  $\hat{W}$ ) and minimizes the *perpendicular* distance to the linear fit. PCA is one of the methods that can be used to solve the linear TLS problem.

## 6. Conclusions

In this paper PCA is used to detect correlations between different velocity points and different spectral lines. The first principal component can be used to detect magnetic activity in stars. But the most important application of PCA is the denoising of individual spectral lines of stellar spectropolarimetric observations. The capabilities of the method are analysed using numerical simulations. By assuming that the contaminating noise presents negligible correlation, we are able to isolate the signal from the noise. We have demonstrated that improvements close to one order of magnitude in the signal to noise ratio per spectral line are typical for the present quality of observed stellar polarised spectra. However, note that, although the method filters the noise in each individual spectral line, the information contained in all of them is taken into account. The increase in the  $S/N$  facilitates the future analysis of individual lines with standard techniques based on polarised radiative transfer theory.

The PCA denoising technique relies only on one free parameter: the number of PCA eigenvectors included in the reconstruction of the signal. We have suggested an automatic criterium for its selection that works well on average. However, better denoising results can be obtained if one carefully analyzes the resulting PCA eigenvectors and only selects those that carry an important amount of signal as compared to the noise.

Although the algebra is different, the PCA denoising technique is, in some way, related to other successful techniques for the detection of magnetic signals in stars as the line addition technique (Semel & Li, 1996) and the LSD procedure (Donati et al., 1997). Since we use the cross-product matrix the first principal component is very close to the mean profile obtained with the line addition. Moreover, PCA is directly related to Total Least-Squares, a method that can be seen as a generalization of LSD.

**Acknowledgements.** This research has been partially funded by the Spanish Ministerio de Educación y Ciencia through project AYA2007-63881.

## References

- Asensio Ramos, A., Socas-Navarro, H., López Ariste, A., & Martínez González, M. J. 2007, *ApJ*, 660, 1690
- Carroll, T. A., Kopf, M., Ilyn, I., & Strassmeier, K. G. 2008, *Astron. Nachr.*, 328, 1043
- Christensen-Dalsgaard, J., Hansen, P. C., & Thompson, M. J. 1993, *MNRAS*, 264, 541
- Donati, J.-F., Semel, M., Carter, B. D., Rees, D. E., & Collier Cameron, A. 1997, *MNRAS*, 291, 658
- Donati, P., Catala, C., Landstreet, J. D., Petit, P., & the ESPaDOnS Team. 2007, in *ASP Conf. Ser.*, Vol. 358, *Solar Polarization 4*, ed. R. Casini & B. W. Lites, 362
- Fontenla, J. M., Avrett, E. H., & Loeser, R. 1993, *ApJ*, 406, 319
- Hansen, P. C. 1992, *SIAM Rev.*, 34, 561
- Hansen, P. C., Sekii, T., & Shinahashi, H. 1992, *SIAM J. Sci. Stat. Comput.*, 13, 1142
- Hansen, P. C., & O’Leary, D. P. 1993, *SIAM J. Sci. Stat. Comput.*, 14, 1487
- Huffel, S. V. & Lemmerling, P. 2002, *Total Least Squares and Errors-in-Variables Modeling: Analysis, Algorithms and Applications* (Dordrecht, The Netherlands: Kluwer Academic Publishers)
- Landolfi, M., Landi degl’Innocenti, E., Landi degl’Innocenti, M., & Leroy, J. L. 1993, *A&A*, 272, 285
- Loève, M. M. 1955, *Probability Theory* (Princeton: Van Nostrand Company)
- Petit, P. 2007, in *ASP Conf. Ser.*, Vol. 358, *Solar Polarization 4*, ed. R. Casini & B. W. Lites, 335
- Press, W. H., Teukolsky, S. A., Vetterling, W. T., & Flannery, B. P. 1986, *Numerical Recipes* (Cambridge: Cambridge University Press)
- Semel, M., Rees, D. E., Ramírez Vélez, J. C., Stift, M. J., & Leone, F. 2006, in *ASP Conf. Ser.*, Vol. 358, *Solar Polarization 4*, ed. R. Casini & B. W. Lites, 355
- Semel, M. 1989, *A&A*, 225, 456
- Semel, M. & Li, J. 1996, *Sol. Phys.*, 164, 417